PAPER

Effect of grain size on the behavior of hydrogen/helium retention in tungsten: a cluster dynamics modeling

To cite this article: Zhe Zhao *et al* 2017 *Nucl. Fusion* **57** 086020

IOP Publishing | International Atomic Energy Agency Nuclear Fusion

Nucl. Fusion **57** (2017) 086020 (10pp) https://doi.org/10.1088/1741-4326/aa7640

Effect of grain size on the behavior of hydrogen/helium retention in tungsten: a cluster dynamics modeling

Zhe Zhao[1,2], Yonggang Li[1,3], Chuanguo Zhang[1], Guyue Pan[1,3], Panfei Tang[1,3] and Zhi Zeng[1,3]

[1] Key Laboratory for Materials Physics, Institute of Solid State Physics, Chinese Academy of Sciences, Hefei 230031, People's Republic of China
[2] School of Physics and Material Science, Anhui University, Hefei 230601, People's Republic of China
[3] University of Science and Technology of China, Hefei 230026, People's Republic of China

E-mail: ygli@theory.issp.ac.cn and zzeng@theory.issp.ac.cn

Received 4 March 2017
Accepted for publication 1 June 2017
Published 28 June 2017

Abstract

Reducing ion retention in materials is a key factor in the management of tritium inventory, the selection of compatible plasma-facing materials (PFMs), and thus the future development of fusion reactors. In this work, by introducing the cellular sink strength of grain boundaries (GBs) into the cluster dynamics model, the behavior of hydrogen (H) and helium (He) retention in W with different grain sizes is studied under various irradiation conditions systematically. It is found that the H/He retention increases dramatically with decreasing grain size at typical service temperatures, due to the enhancement of H/He capture ratio by GBs. Generally, He retention exists in three forms: He in GBs, in dislocations and in clusters (He_mV_n, He_n and He_nI). Our further study shows that, under the irradiation of low energy and low fluence ions, the contribution of He in clusters is negligible. The total He retention is thus dominated by the competing absorption of GBs and dislocations, that is, changing from the dislocation-based to grain boundary-based retention with decreasing grain size.
H retention also presents the same behavior. In view of these grain size-related behaviors of H/He retention in W, it is suggested that coarse-grained crystals should be selected for W-based PFMs in practice.

Keywords: cluster dynamics model, H/He retention, grain size, grain boundaries, dislocations

(Some figures may appear in colour only in the online journal)

1. Introduction

In tokamak fusion reactors like ITER, plasma-facing materials (PFMs) are subjected to up to 20 MW m^{-2} high heat loads, 14.1 MeV neutrons as well as intensive fluxes of energetic hydrogen isotopes (H, D and T) and helium (He) from D–T fusion reaction [1]. Plasma–surface interaction (PSI) can induce significant large quantity of defects and strong disruption in crystal structures, and further cause serious surface damage like erosion, sputtering and blistering [2]. Especially, H/He atoms injected into metals would be deeply trapped by inherent defects such as voids, precipitates, grain boundaries (GBs) and dislocations. The accumulation of H/He in the free volume of intrinsic defect changes the surface microstructures and morphologies, which further aggregate more H/He retention in PFMs [3, 4]. Therefore, compatible PFMs should be selected to combat these critical issues. Due to its high-melting point, excellent thermal conductivity, low tritium retention and low sputtering yields, tungsten (W) has been regarded as one of the most promising candidates for divertor armor in future fusion reactors [5]. Many attentions have been paid to the H/He irradiation response of W under various burning plasma conditions [6–18]. While further efforts are still needed to understand especially the behavior of H/He retention in W-based PFMs.

Different methods are employed to improve the radiation resistance of W-based PFMs, such as, doping impurities, grain refining and alloying. In particular, it was predicted that nano-crystalline (NC) materials could present higher radiation resistance compared to their coarse-grained (CG) counterparts under certain conditions, due to the high density of GBs that can act as an efficient venues for reducing the accumulation of intrinsic defects in grain interior [19–23]. Even though experiments have not observed/reported H atoms or bubbles accumulated in GBs, related atomistic simulations (like molecular dynamics and density functional theory) found that H preferentially migration towards and could be strongly trapped in GBs [24–26]. The deviations between experiments and atomistic simulations could be caused by that the binding energies between H or vacancy and H_mV_n clusters decrease with increasing size [27], and only amount of small H bubbles form that beyond the resolution of TEM. In contrast, experiments shew that He atoms intend to accumulate at interfaces/GBs and grow into larger bubbles, with less He retention and damages left in grain interior [28, 29]. However, the grain size on the total ion retention and degradation of material mechanical properties are still unclear and even controversial. It is crucial to investigate the H/He retention behavior in W with considering the effect of GBs and reveal the relationship between H/He retention and grain size.

In recent years, some experimental [9, 14–16, 28–30] and theoretical [24, 26, 27, 31] researches have been performed to study the behavior of H/He retention in NC W. González *et al* [9] pointed out that nanostructured W with a large number of interfaces retained more H than coarse-grained W samples. Ogorodnikova *et al* [14–16] found that the D retention for thin nanostructured produced by combined magnetron-sputtering and ion implantation technique is significantly higher than that of poly-crystalline. El-Atwani *et al* [28, 29] studied the formation of He bubbles in W with different grain sizes by TEM and found that larger facetted bubbles occurred on NC grains. 't Hoen *et al* [30] observed that D retention increases with decreasing crystalline size. Related atomistic simulations have also been performed to reveal the micro-mechanisms of H/He trapping in W bulk [32, 33]. Piaggi *et al* [24] investigated the effect of nanometer grain size on H diffusion coefficient in W by the molecular dynamics (MD) method and found a lower diffusion coefficient in NC W than that in CG W. Chen *et al* [26] demonstrated that embedding H/He atoms facilitates grain boundary (GB) sliding and intergranular fracture. Generally, it is difficult for atomistic methods to deal with the defect behavior over at least four orders of grain size, due to the limitation of time- and space-scale. Thus, it is necessary to further develop the meso-scale methods like the object kinetic Monte Carlo (OKMC) and cluster dynamics (CD) models. Becquart *et al* [34, 35] developed an OKMC model to simulate the dynamics of He and point defects in single-crystalline tungsten (SC W). Valles *et al* [27, 31] used the open-source OKMC code (MMonCa) to discuss the H/He behavior in NC W and SC W, and pointed out that an enhancement of H/He retention in NC W. While typically OKMC cannot deal with defect evolution in the intermediate-range of grain size between hundred-nm NC and infinite crystal. Meanwhile, CD has also been employed to study the depth-distribution of H/He ion retention in SC and CG W/Be (beryllium) bulk [36–45] under different conditions. However, the effect of grain size on H/He retention in W, from nm to infinite, has still not been studied systematically.

In this paper, we develop a CD model by taking account of GB sink strength to investigate the effect of grain size on H/He retention in W under low fluence ion irradiation at typical temperatures 300 K and 873 K, by the advantages of no restriction in time and space. Our results will improve the understanding of H/He ion retention in PFMs under fusion relevant conditions.

2. Theoretical model

The dynamics evolution of defects in materials is a long-time, multi-scale and multi-micromechanisms coupling process, including defect production, diffusion and reaction. Our group has established a sequential multi-scale modeling approach to describe these processes by combining the Monte Carlo (IM3D [46]), atomistic (DFT and MD) and CD (IRadMat [41, 42]) models. The spatial distribution of primary radiation damage is calculated with IM3D Monte Carlo code [46, 47]. The long-time evolution of defects can be simulated with IRadMat, a deterministic CD model we developed based on the mean-field rate theory. This scheme has been successfully applied on H/He retention in poly-crystalline W/Be under different irradiation conditions (such as ion energy, flux, fluence and temperature) [41–45], and the mechanisms of H embrittlement in iron [48]. Here, by introducing the cellular sink strength of GBs into IRadMat, we can take into account the effect of grain size on the behavior of H/He retention in W.

2.1. Master equations

The defect dynamical processes considered in the present work are described by the rate theory model in terms of the concentration of different defects, for the case of synergistic effects of ion implantation and neutron irradiation. The evolution of different types of defects is described in a set of one-dimensional diffusion-reaction equations by considering their diffusion process of mobile defects along with depth and possible reactions with other defects, as given by the master equations [41–45],

$$\frac{\partial C_\theta}{\partial t} = G_\theta + D_\theta \nabla^2 C_\theta + \sum_{\theta'} [\omega(\theta', \theta) C_{\theta'} - \omega(\theta, \theta') C_\theta] - L_\theta, \quad (1)$$

where C_θ is the concentration of defect θ in the irradiated system at a specific depth and time. The basic types of defects θ included in the model for hydrogen (H) and helium (He) in W, which are self-interstitial atoms (SIAs, denoted as I), vacancies (V), hydrogen/helium atoms (H/He) and their formed complex clusters ((I_n, V, H, HI, H_mV) and (I_n, V_n, He_n, He_nI, and He_mV_n) for H and He, respectively), where m and n are the numbers of defects in a loop/cluster. Inherent defects like grain boundaries (GBs) and dislocation lines (DLs) are

Table 1. Parameters used for H and He irradiated on W.

	Symbol	Value	References
Lattice constant	a_0	3.1652 Å	[52]
Recombination	r_{IV}	4.65 Å	[42]
Dislocation line density	ρ_{D}	10^{12} m^{-2}	[53]
SIA pre-exponential factor	D_{I_0}	10^{-8} m^2 s^{-1}	[49, 50]
V pre-exponential factor	D_{V_0}	10^{-4} m^2 s^{-1}	[45]
H pre-exponential factor	D_{H_0}	4.1×10^{-7} m^2 s^{-1}	[54]
Migration energy of V	$E_{\mathrm{V}}^{\mathrm{m}}$	1.66 eV	[55]
Migration energy of SIA	$E_{\mathrm{I}}^{\mathrm{m}}$	0.013 eV	[55]
Migration energy of H	$E_{\mathrm{H}}^{\mathrm{m}}$	0.39 eV	[56]
Formation energy of V	$E_{\mathrm{V}}^{\mathrm{f}}$	3.8 eV	[57]
Formation energy of SIA	$E_{\mathrm{I}}^{\mathrm{f}}$	9.466 eV	[57]
Formation energy of H	$E_{\mathrm{H}}^{\mathrm{f}}$	2.45 eV	[55]
Binding energy of I_2	$E_{\mathrm{I}_2}^{\mathrm{b}}$	2.12 eV	[35]
Binding energy of H-I	$E_{\mathrm{H\text{-}I}}^{\mathrm{b}}$	0.33 eV	[34]
Binding energy of HV	$E_{\mathrm{H\text{-}V}}^{\mathrm{b}}$	1.18 eV	[58]
He pre-exponential factor	D_{He_0}	10^{-8} m^2 s^{-1}	[35]
Migration energy of He	$E_{\mathrm{He}}^{\mathrm{m}}$	0.06 eV	[59]
Formation energy of He	$E_{\mathrm{He}}^{\mathrm{f}}$	4.0 eV	[35]
Binding energy of V_2	$E_{\mathrm{V}_2}^{\mathrm{b}}$	0.6559 eV	[60]
Binding energy of He_2	$E_{\mathrm{He}_2}^{\mathrm{b}}$	1.02 eV	[35]
Binding energy of He_n-I	$E_{\mathrm{He}_n\text{-I}}^{\mathrm{b}}$	0.94 eV	[35]
Binding energy of He_mV_n-I	$E_{\mathrm{He}_m\mathrm{V}_n\text{-I}}^{\mathrm{b}}$	0.7 eV ($m > 6$)	[61]

also included in the model. In practice, only SIAs (I), di-interstitials (I_2), V and H/He are considered to be mobile for simplification, while all other defect clusters are considered to be immobile. For mobile defects, the terms of equation (1) are defined as follows. G_θ is the production rate. D_θ represents the diffusion coefficients ($D_\theta = D_{\theta_0}\exp(-E_\theta^{\mathrm{m}}/K_{\mathrm{B}}T)$, where D_{θ_0} is pre-exponential factor, E_θ^{m} is migration energy and K_{B} is Boltzmann constant). L_θ represents inherent absorption rate ($L_\theta = K_{\mathrm{GB}}^\theta D_\theta C_\theta + K_{\mathrm{DL}}^\theta D_\theta C_\theta$, where K_{GB}^θ and K_{DL}^θ are set as the sink strength of GBs and DLs, respectively). $\omega(\theta', \theta)$ is the transition rate coefficient per unit concentration of type θ' defect cluster transforming into type θ defect cluster. The corresponding reaction types for H and He in W are set as the same as in our previous researches [41, 42], respectively, which have reasonably described the behavior of H/He retention in W bulk for synergetic ion and neutron irradiation. All parameters for H and He in W are carefully determined from the published values by experiments or DFT/MD calculations, and typical data are listed in table 1.

The first-order boundary condition ($C(z = 0) = 0$, where z is the depth) is reasonably selected for considering the behavior of H/He desorption from surfaces. In order to further decrease the computational cost, the Fokker–Planck approximation is adopted in our model to transform these discrete master equations into continuous equations based on the Taylor expansion to the second term [49, 50]. Here, the set of ordinary differential equations (ODEs) is solved by using *lsoda* subroutine package [51].

2.2. Sink strength of GBs and DLs

GBs and DLs are the significant sinks of mobile defects during irradiation and thus the loss of mobile defects at such sinks must be quantitatively determined by considering the sink strength of GBs and DLs. Various expressions for the sink strength of GBs have been given by using either the so-called embedding [62] or cellular model [63]. Bullough had compared these two types of sink strength by GBs in much detail, and argued that the cellular sink strength is the preferable one for regular distributed GBs [64]. Thus, it is reasonable for us to select the cellular sink strength model to describe the uniform distributed GBs here. The absorption processes of mobile defects by GBs is described as $\theta + \mathrm{GB} \rightarrow \mathrm{GB} - \theta$, $\theta = \mathrm{I, V, H, He}\ \ldots$, whose sink strength is given by [63, 64],

$$K_{\mathrm{GB}}^\theta = S_{\mathrm{m}}^\theta \left(\frac{\sqrt{S_{\mathrm{m}}^\theta}\, d}{2} \coth \frac{\sqrt{S_{\mathrm{m}}^\theta}\, d}{2} - 1 \right) \times \left(1 + \frac{S_{\mathrm{m}}^\theta d^2}{12} - \frac{\sqrt{S_{\mathrm{m}}^\theta}\, d}{2} \coth \frac{\sqrt{S_{\mathrm{m}}^\theta}\, d}{2} \right)^{-1}, \quad (2)$$

where S_{m}^θ represents the total sink strength of the medium (including defect clusters, loops and DLs) without the GBs and surfaces, and d is the diameter of a spherical grain. For a single crystal, the value of GB sink strength is set to zero. Generally, the binding energies of mobile defects (I, V and H/He) with GBs are usually much higher than the ones with defect clusters for W. For example, the calculated binding energies of SIAs with a typical tilt symmetric GB in W is as high as 7.5 eV [65]. And the average binding energy of H in GBs for randomly oriented grains in W is calculated to be at least 2.0 eV [24]. Meanwhile, as shown in the experiment, GBs also act as strong traps for sequestering He [66]. Thus, the emitting of mobile defects from GBs is neglected in the CD model, which is reasonable enough at least for the cases of low ion fluences or low temperatures. In fact, excluding the insignificant desorption ratio of mobile defects from GBs could not affect the exact restriction relation of ion retention due to GB absorption, as discussed below.

In addition, we consider a uniform distribution of dislocation line (DL) density with the corresponding sink strength [67],

$$K_{\mathrm{DL}}^\theta = \rho Z_{\mathrm{DL}}^\theta, \quad (3)$$

where ρ is the DL density in the material, Z_{DL}^θ is a dimensionless factor which represents the absorption efficiency of point defects by DLs related to the defect-dislocation elastic interaction, which is usually set as $Z_{\mathrm{DL}}^I = 1.2$, $Z_{\mathrm{DL}}^V = 1.0$ and $Z_{\mathrm{DL}}^{\mathrm{H}} = Z_{\mathrm{DL}}^{\mathrm{He}} = 1.0$, respectively. Under the same consideration as for GBs, the emitting of defects from DLs is also neglected in a reasonable approximation.

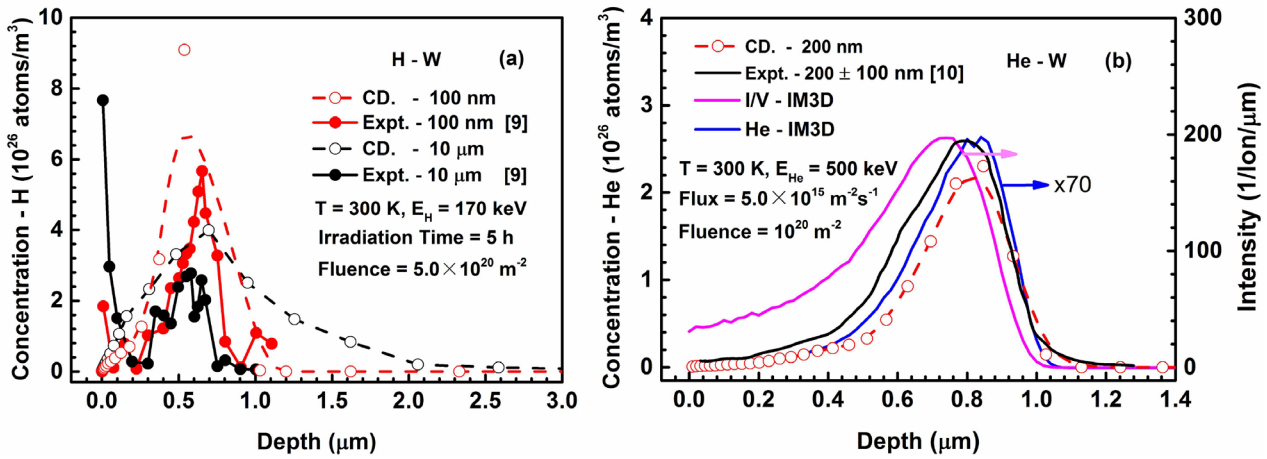

Figure 1. Verification of the CD model with experiments [9, 10]. (*a*) The depth distribution of H concentration in W under H ion irradiation with the energy of 170 keV and the fluence of 5.0×10^{20} m^{-2} at 300 K; (*b*) the depth distribution of He concentration in W under He ion irradiation with the energy of 500 keV and the flux of 5.0×10^{15} m^{-2} s^{-1} up to fluence of 1.0×10^{20} m^{-2} at 300 K. (*a*) Reproduced courtesy of IAEA. Figure from [9]. Copyright 2015 IAEA. (*b*) Reprinted from [10], Copyright 2007, with permission from Elsevier.

3. Results and discussion

3.1. Verification of the CD model with experiments

The CD model used in the present work is verified by comparing with experimental results [9, 10] directly. The depth distribution of H retention in W with the grain size of 100 nm and 10 μm as well as He retention in W with the grain size of 200 nm are shown in figure 1. The simulation conditions for H/He ion irradiation are set as following: 170 keV H ions with the fluence of 5.0×10^{20} m^{-2} and 500 keV He ions with the flux of 5.0×10^{15} m^{-2} s^{-1} up to a fluence of 1.0×10^{20} m^{-2} at room temperature, respectively. The depth distribution of primary radiation damage (H/He atoms and *dpa*) in W was calculated by IM3D code [43], and used as the initial distribution of point defects for CD calculations. As an example, we only showed the primary depth distribution for He in W as given in figure 1(*b*). Both for H and He, the CD calculation results are consistent with the experimental ones well, which confirms the accuracy of our model.

Trapping and diffusion are the two main effects controlling the depth distribution profiles of H/He retention in W. The competition of these two effects results in the profiles with a peak at about 690 nm for H and 800 nm for He, respectively, and a long tail beyond the projected range. Comparing to the experiments [9, 10], the calculated concentration is somewhat overestimated and underestimated especially near the peak for H and He in W, respectively, which can be caused by some secondary factors. On the one hand, for H in W (figure 1(*a*)), high H concentration in sub-surface observed in the experiment is mainly due to the enhanced accumulation in surface microstructures (like voids, bubbles, DLs and impurities) and the morphology reconstruction under H ion erosion. The enhanced absorption of H on the surface will surely decrease the amount of H retention in bulk correspondingly as in the experiment. For He in W (figure 1(*b*)), the mean value of 5.0×10^{15} m^{-2} s^{-1} used in the simulation instead of an uncertain flux ranging from 10^{15} to 10^{16} m^{-2} s^{-1} in the experiment may overestimate the annealing time and thus He desorption, which causes a lower calculated He retention comparing to the experimental one especially at the peak. On the other hand, several approximations made in the model would also introduce deviations more or less, such as, the neglecting of the emission of mobile defects from GBs and DLs and the immobile of small clusters (X_mV_n, X_m, and X_mI, X = H/He). In addition, CD cannot intrinsically account for spatial correlations between Frenkel pairs in cascades [68]. It would underestimate the contribution of He retention by vacancies, due to the decreased vacancy concentration caused by lower I-V recombination probability. However, the main features of grain size-dependent H/He retention in W under the certain conditions mentioned should be not influenced by these approximations. Besides, our previous researches [41–45] about ion retention in W/Be have also verified our CD by comparing experiments, for example, [11–13]. Thus, by further taking account of the GB sink strength, the CD model can naturally simulate the effect of grain size on H/He retention in W under certain irradiation conditions that H/He accumulation in GBs is unsaturated or H/He desorption from GBs is negligible.

3.2. H/He retention and depth distribution in W

The total concentration for both H and He retention in W under different grain sizes at two temperatures (typically room temperature and ITER service temperature 873 K) are obtained as shown in figure 2. It can be found that regardless of temperature and ion fluence, H/He retention has been enhanced dramatically with decreasing grain size. Two critical factors contribute to the higher H/He retention in NC W, that is, the high trapping rate with high density of GBs and the fast diffusion of H/He with the relatively low migration energies (0.39 eV for H and 0.06 eV for He) in W. When GBs vanishing, H/He retention in SC W is at the lowest level, which is mainly contributed by the trapping of vacancies and DLs.

Furthermore, the values of H/He retention at 873 K are lower than those at room temperature. On the one hand, the H/He retention exists in three forms, H/He in GBs, DLs and in clusters (mainly H, HI, H_mV_n for H and He_n, He_nI, He_mV_n for He).

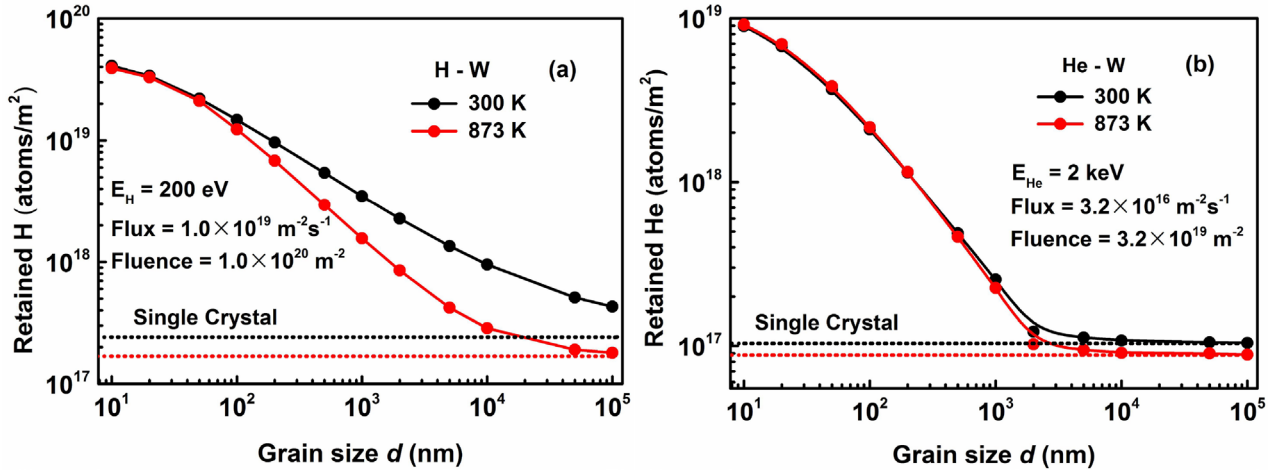

Figure 2. Grain size dependence of (*a*) total H retention in W under H ion irradiation with the energy of 200 eV and fluence of 1.0×10^{20} m^{-2} and (*b*) total He retention in W under He ion irradiation with the energy of 2 keV and fluence of 3.2×10^{19} m^{-2}.

Due to binding energy of H/He with clusters is smaller [27], thus, the H/He desorption is mainly contributed by H/He dissociation (essentially from H/He clusters) and will be enhanced when the temperature increases to 873 K. On the other hand, the difference in grain size-based H/He retention at different temperatures is more obvious for H (figure 2(*a*)) than for He (figure 2(*b*)), which is mainly because the system of H in W cannot quickly reach the equilibrium state at room temperature with the higher migration energy of 0.39 eV in contrast to that of He (0.06 eV). But according to figure 2(*b*) the accumulation of He in NC W does not noticeably change with increasing sample temperature from 300 K to 873 K. On the one hand, the low fluences of 3.2×10^{19} m^{-2} for He ion irradiated W is used in the present CD calculations, which can be quickly absorbed by inherent defects (GBs, DLs, vacancies) especially in NC W due to enough high density of trapping sites provided by GBs. On the other hand, the lower ion fluences induce less vacancies and the concentration of He_mV_n clusters is a minor part compared to that He trapped by GBs and DLs, which will also have less influence on the amount of He dissociation from He clusters at 300 K and 873 K. In contrast, the difference between 300 K and 873 K becomes obvious when the grain size increased to coarse-grained range, due to the effect of temperature on the amount of He dissociation from He clusters becomes more obvious with the decrease of GB density and the corresponding lower He atom trapping.

The behavior of H/He retention increasing with decreasing grain size is also consistent with the experiments of H/He retention in different W crystallite sizes [9, 14–16, 30]. In general, high H/He concentration reduces vacancy formation energy in W and thus increases the probability of bubble nucleation and the embedded H/He atom concentration [69]. Embedding H/He atoms facilitates GB sliding and intergranular fracture, and increases the strain rate sensitivity [26]. Therefore, the improving of the radiation tolerance of W via the control of grain size should take account of the high H/He retention in NC W.

Another interesting phenomenon shown in figure 2(*b*) is that the He retention in W at grain size of about several-μm is nearly equal to the value in single crystal. It is mainly because He trapped in GBs decreases to nearly the same level of other sinks (such as DLs and voids), that is, the enhancement of He retention contributed by GBs vanishes at the grain size beyond of several-μm. The contributions of different He forms to He retention in W under different grain sizes will be discussed below.

In order to understand the grain size dependent H/He retention behavior in more detail, the depth and grain size dependence of H/He concentration in W at 300 K are given in figure 3. The depth region of H/He retention can be tentatively divided into two zones according to their respect features, that is, a dramatic increase in the near-surface layer and a rapid decline along depth in the bulk. For grain size in tens-nm, there is a peak at several-nm below surface for both H and He in W, which is mainly due to the enhanced absorption of H/He atoms by high-density GBs at near surface. High density of GBs also reduces the diffusion of H/He into depth and causes the rapid decrease of H/He retention along with depth. Moreover, the depth range of H/He retention extends deeply into bulk with increasing grain size, which is mainly due to the decrease of H/He trapping in GBs. The behaviors of H and He depth distribution are somewhat different, that is, the range of H concentration peak extends into bulk with increasing grain size (figure 3(*a*)), while He tends to self-accumulate at subsurface even at grain sizes of several-μm (figure 3(*b*)).

For that the grain size-dependent behavior of H and He retention in W is similar under low ion fluence irradiation, we take He–W system as an example to discuss the contribution of He forms to He retention in W, under He ion irradiation with the energy of 2.0 keV and flux of 3.2×10^{16} m^{-2} s^{-1} up to 3.2×10^{19} m^{-2} at 873 K. He retention in W is mainly contributed by three forms, that is, the trapping in He clusters (like He_mV_n, He_n and He_nI), GBs and DLs. Here we count He clusters as the summation of the different types of He clusters at different depths. The depth distribution of total He atoms as well as different He forms in W for grain size of 50 nm, 10 μm and 100 μm are shown in figure 4. For grains in all sizes concerned in the present work, the concentration of He clusters is a minor part in contrast to that of He trapped in GBs and

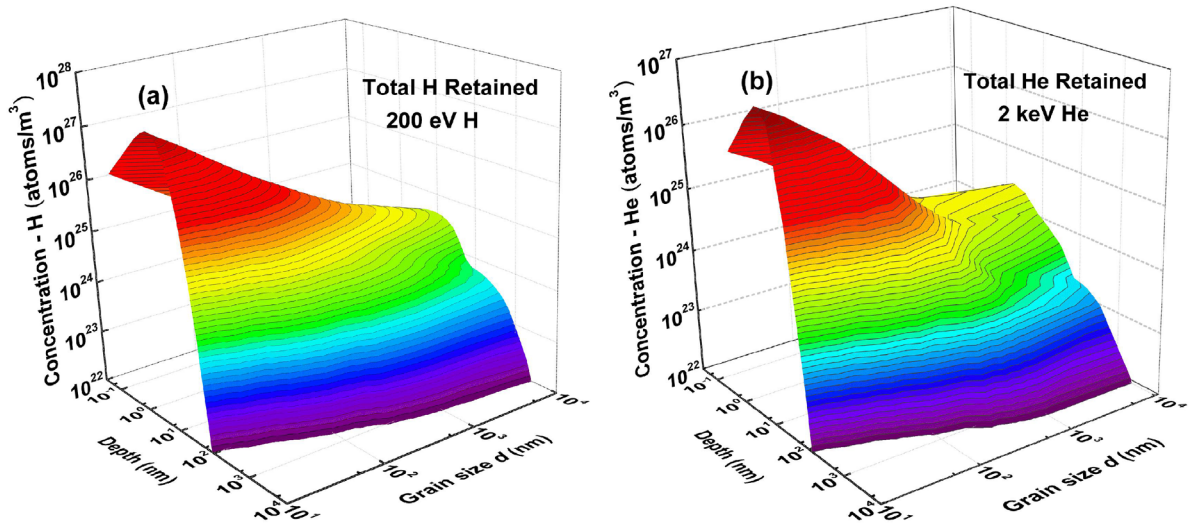

Figure 3. Depth and grain size dependence of (*a*) H concentration in W under H ion irradiation with energy of 200 eV and fluence of 1.0×10^{20} m^{-2}, and (*b*) He concentration in W under He ion irradiation with the energy of 2 keV and fluence of 3.2×10^{19} m^{-2} at 300 K.

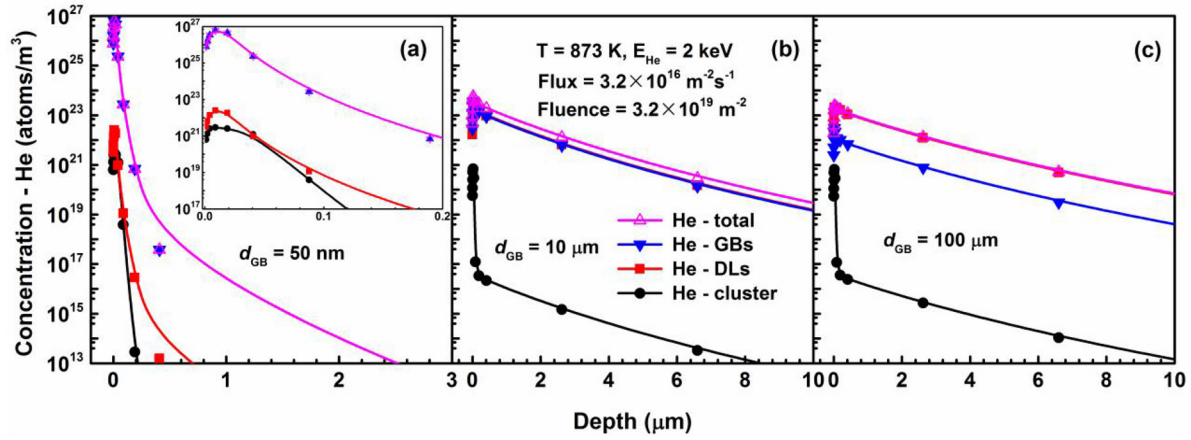

Figure 4. Depth dependence of He concentration for different He forms under He ion irradiation with the energy of 2.0 keV and flux of 3.2×10^{16} m^{-2} s^{-1} up to fluence of 3.2×10^{19} m^{-2} on W at 873 K, for different grain sizes of (*a*) 50 nm, (*b*) 10 μm and (*c*) 100 μm, respectively.

DLs. Seen in figure 4(*a*), at grain size of 50 nm, He trapped in GBs contribute nearly all of He concentration in W, while He trapped in DLs is a minor part. Thus, high density GBs in NC materials enhances ion retention dramatically even though it is termed as an effective way to suppress defect accumulation. When grain size increasing to 10 μm, He concentration trapped in GBs and DLs are comparable (about 48% and 51% in GBs and DLs, respectively (figure 4(*b*)), which changes He retention from grain boundary-based to dislocation-based form. At grain size of 100 μm, He concentration trapped by DLs dominates He retention in W (figure 4(*c*)), that is, about 93% in DLs and 6% in GBs.

In order to theoretically analyze the restrictive correlation of He trapped in GBs and DLs, the ratio of He concentration trapped in GBs to that in DLs with grain size are given as in figure 5. The ratio calculated by CD (black dots) decreases linearly at first with increasing grain size but deviates the linear relationship with the grain size increasing beyond several-μm. It can be explained by a chemical rate theory that incorporates GB and dislocation sink strength. The time-dependence of He concentration trapped in GBs and DLs can be described as,

$$\begin{aligned}\frac{\partial C_{\text{GB-He}}}{\partial t} &= K_{\text{GB}}^{\text{He}} D_{\text{He}} C_{\text{He}}.\\ \frac{\partial C_{\text{DL-He}}}{\partial t} &= K_{\text{DL}}^{\text{He}} D_{\text{He}} C_{\text{He}}.\end{aligned} \tag{4}$$

Thus, the ratio of He concentration trapped in GBs and DLs is determined by the sink strength of GBs and DLs directly,

$$\frac{C_{\text{GB-He}}}{C_{\text{DL-He}}} = \frac{K_{\text{GB}}^{\text{He}}}{K_{\text{DL}}^{\text{He}}}. \tag{5}$$

Due to that the concentration of He clusters is a minor part in all range of grain size under the irradiation of low energy, low fluences (figure 4), the total sink strength without the GBs and surfaces in equation (2) $S_{\text{m}}^{\text{He}} \approx K_{\text{DL}}^{\text{He}} = \rho Z_{\text{DL}}^{\text{He}}$, where the sink strength of DLs (K_{DL}^{θ}) is given as equation (3). For small grains and low internal sink strengths in grains ($\sqrt{S_{\text{m}}^{\text{He}}}\, d \to 0$), $K_{\text{GB}}^{\text{He}} = 57.6/d^2$, which is proportional inversely to the square of grain diameter d [70]. The ratio of He concentration trapped in GBs to that in DLs can be estimated as,

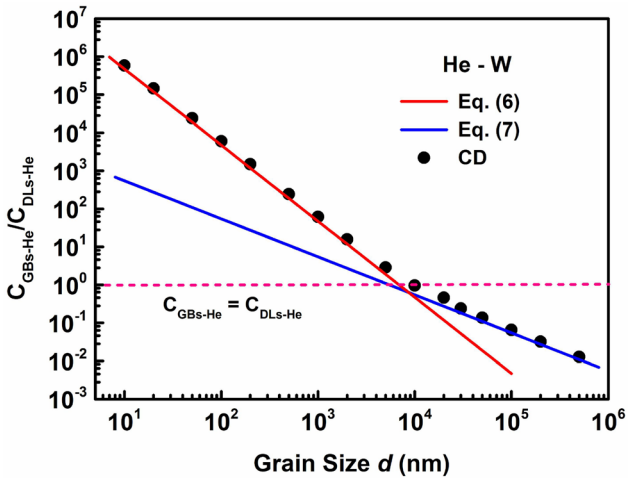

Figure 5. Ratio of He concentration trapped in GBs to that in DLs with grain size for W under 2.0 keV He ion irradiation with a flux of 3.2×10^{16} m^{-2} s^{-1} up to the fluence of 3.2×10^{19} m^{-2} at 873 K. The asymptotic curve of equations (6) and (7) are shown as the red solid line and the blue solid line, respectively.

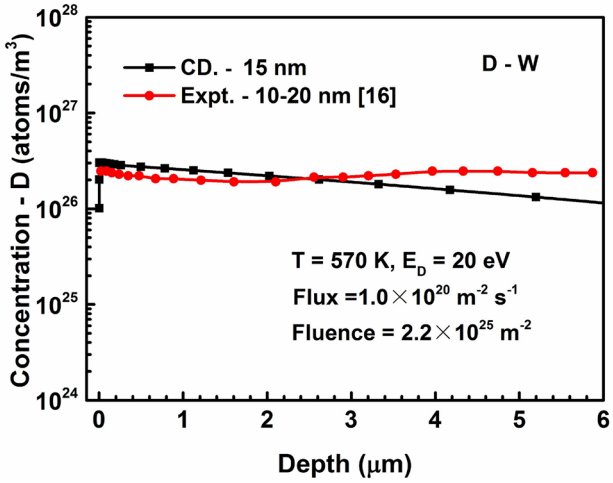

Figure 6. Verification of the CD model with experiment [16]. The depth distribution of D concentration in nanostructured W (with the grain size of 15 nm) under D ion irradiation with the energy of 20 eV and fluence of 2.2×10^{25} m^{-2} at 570 K. Reprinted from [16], Copyright 2013, with permission from Elsevier.

$$\frac{C_{\text{GB-He}}}{C_{\text{DL-He}}} = \frac{57.6}{d^2 \rho Z_{\text{DL}}^{\text{He}}}. \tag{6}$$

At another limit, for large grains and high internal sink strengths in grains ($\sqrt{S_{\text{m}}^{\text{He}}}\, d \to \infty$), $K_{\text{GB}}^{\text{He}} = 6\sqrt{S_{\text{m}}^{\text{He}}}/d$, the ratio is then,

$$\frac{C_{\text{GB-He}}}{C_{\text{DL-He}}} = \frac{6\sqrt{S_{\text{m}}^{\text{He}}}/d}{\rho Z_{\text{DL}}^{\text{He}}} \approx \frac{6}{d\sqrt{\rho Z_{\text{DL}}^{\text{He}}}}. \tag{7}$$

Two asymptotic relationships (equations (6) and (7)) between $C_{\text{GB-He}}/C_{\text{DL-He}}$ and d are also given as in figure 5. The ratio simulated by CD (black dots) is consistent with the linear relationship of equation (6) (red line) with the grain size below several-μm, while converts to another linear relationship of equation (7) (blue line) with grain size beyond several-μm. The coincidence between simulation and theoretical prediction also proves the accuracy of our CD model through introducing the cellular sink strength of GBs to investigate H/He retention in W with different grain sizes. Thus, under the irradiation of low energy and low fluence ion beams (H/He undersaturation), H/He retention in W with different grain sizes are mainly dominated by two different mechanisms, namely, the grain boundary-based and dislocation-based retention for NC W and CG W, respectively. However, when irradiation conditions change to high energy, high fluence ion beams (H/He super-saturation), the contribution of H_mV_n/He_mV_n clusters to H/He retention will be enhanced no longer a minor part in contrast to that of trapped in GBs and DLs.

3.3. Extend application of the CD model for high ion fluences

Typically, the cellular sink strength model used here has not included the emission of mobile defects from GBs, which is valid when H/He accumulation in GBs is unsaturated or H/He desorption from GBs is negligible. It is meaningful to select low ion fluences to systematically investigate the influence of grain size on H/He retention in W as given above. While for practical fusion conditions, low-energy, high fluence ions are usually performed to bombard W-base PFMs, thus, the effect of H/He emission from GBs becomes obvious and should be additionally considered in our CD model. By simply describing the emission of D from GBs and DLs with an empirical trapping energy of 0.85 eV [16], the simulated depth-distribution of D retention in nanostructured W (grain size of 15 nm), under low energy (20 eV), high fluence (2.2×10^{25} m^{-2}) D ion irradiation at 570 K, is compared with experimental one directly, as shown in figure 6. In this calculation, a lower D ion migration energy of 0.21 eV is reasonably selected for considering the sample with lower atomic density. By considering D desorption from GBs and DLs, the CD calculated result can catch the main features of experimental measurement [16] in several respects, that is, a minor peak in the near surface (tens-nm) and a nearly platform in the sub-surface (tens-nm to 2 μm) for the depth distribution profiles of D in W. There are also some deviations like a higher concentration of D ions with a slowly decline along depth by CD rather than an almost constant in experiments. The simulation conditions deviate more or less from the experimental details, like the DL density, crystal orientation and W atomistic density, which may influence the migration energy of D ions. Thus, the emission of mobile defects (especially for H and He) for inherent defects (like GBs and DLs) should be included at least for NC W under high fluence ion irradiation. Meanwhile, we could understand the extension to high ions fluences from the well established mechanism of GBs trapping defects, in which the grain boundary density will increase dramatically with decreasing grain size, and the ions absorbed by GBs will be naturally enhanced with decreasing grain size even under high ion fluences or ion saturation. Thus it is certainty that the tendency that H/He retention enhances dramatically with decreasing grain size in W should be identical under certain conditions and could be extrapolated to more

realistic irradiation conditions (even for high temperature and high fluence). Studies and predictions of the grain size effect on H/He retention in PFMs in realistic plasma conditions will be performed in further work, which also requires the supports from the studies in related atomistic methods.

4. Conclusions

A cluster dynamics model based on the mean-field rate theory has been improved by introducing the cellular sink strength of GBs. The behavior of both H and He retention in W with different grain sizes is investigated systematically, under typical service conditions in fusion devices. H/He retention increases dramatically with decreasing grain size, due to the enhancement of H/He trapped in GBs. Under low energy and low fluence He irradiation, the concentration of He trapped in clusters (He_mV_n, He_n and He_nI) is a minor part comparing to that in GBs and DLs, both in nano-crystalline W and coarse-grained W crystals. Thus, the total He retention is mainly contributed by the competing absorption of GBs and DLs, that is, the grain boundary-based retention for grain size below several-μm while the dislocation-based retention for grain size beyond of tens-μm, at least for low energy and low fluence ion irradiation. Additionally, the D retention in nano-crystalline W by considering D desorption from GBs and DLs in cluster dynamics model are also consistent with experiments under low energy, high fluences D ion irradiation. The tendency of H/He retention in W with different grain sizes should be identical under certain conditions, and could be extrapolated to more realistic irradiation conditions (even for high temperature and high fluence). It is certainly helpful for the understanding and engineering of the radiation tolerance of W via the control of grain size, where the enhancement of H/He retention in nano-crystalline W must be taken into account. In view of this, it is recommended that for W based PFMs coarse-grained crystals should be selected in practice.

Acknowledgments

This work was supported by the National Science Foundation of China under Grant Nos. 11534012, 11475215, 11605231. The Youth Innovation Promotion Association of CAS under Grant No. 2016386, and Director Grants of CASHIPS. Part of the calculations were performed at the Center for Computational Science of CASHIPS, the ScGrid of Supercomputing Center, and the Computer Network Information Center of the Chinese Academy of Sciences. This research work is also supported Tianhe-2JK computing time award at the Beijing Computational Science Research Center (CSRC).

References

[1] Wirth B.D., Nordlund K., Whyte D.G. and Xu D. 2011 Fusion materials modeling: challenges and opportunities *MRS Bull.* **36** 216–22
[2] Gilliam S.B., Gidcumb S.M., Parikh N.R., Forsythe D.G., Patnaik B.K., Hunn J.D., Snead L.L. and Lamaze G.P. 2005 Retention and surface blistering of helium irradiated tungsten as a first wall material *J. Nucl. Mater.* **347** 289–97
[3] Kajita S., Sakaguchi W., Ohno N., Yoshida N. and Saeki T. 2009 Formation process of tungsten nanostructure by the exposure to helium plasma under fusion relevant plasma conditions *Nucl. Fusion* **49** 095005
[4] Sefta F., Hammond K.D., Juslin N. and Wirth B.D. 2013 Tungsten surface evolution by helium bubble nucleation, growth and rupture *Nucl. Fusion* **53** 073015
[5] Loarte A. *et al* 2007 Progress in the ITER physics basis chapter 4: power and particle control *Nucl. Fusion* **47** S203
[6] Tokunaga K., Yoshikawa O., Makise K. and Yoshida N. 2002 Effects of helium irradiation on high heat load properties of tungsten *J. Nucl. Mater.* **307–11** 130–4
[7] Nishijima D., Sugimoto T., Iwakiri H., Ye M.Y., Ohno N., Yoshida N. and Takamura S. 2005 Characteristic changes of deuterium retention on tungsten surfaces due to low-energy helium plasma pre-exposure *J. Nucl. Mater.* **337–9** 927–31
[8] Yoshida N., Iwakiri H., Tokunaga K. and Baba T. 2005 Impact of low energy helium irradiation on plasma facing metals *J. Nucl. Mater.* **337–9** 946–50
[9] González C. *et al* 2015 H trapping and mobility in nanostructured tungsten grain boundaries: a combined experimental and theoretical approach *Nucl. Fusion* **55** 113009
[10] Debelle A., Barthe M.F., Sauvage T., Belamhawal R., Chelgoum A., Desgardin P. and Labrim H. 2007 Helium behavior and vacancy defect distribution in helium implanted tungsten *J. Nucl. Mater.* **362** 181–8
[11] Golubeva A.V., Mayer M., Roth J., Kurnaev V.A. and Ogorodnikova O.V. 2007 Deuterium retention in rhenium-doped tungsten *J. Nucl. Mater.* **363–5** 893–7
[12] Ogorodnikova O.V., Roth J. and Mayer M. 2003 Deuterium retention in tungsten in dependence of the surface conditions *J. Nucl. Mater.* **313–6** 469–77
[13] Alimov V.Kh., Roth J. and Mayer M. 2005 Depth distribution of deuterium in single- and polycrystalline tungsten up to depths of several micrometers *J. Nucl. Mater.* **337–9** 619–23
[14] Ogorodnikova O.V., Sugiyama K., Schwarz-Selinger T., Dürbeck T. and Balden M. 2011 Ion-induced deuterium retention in tungsten coatings on carbon substrate *J. Nucl. Mater.* **419** 194–200
[15] Ogorodnikova O.V., Schwarz-Selinger T., Sugiyama K. and Alimov V. Kh. 2011 Deuterium retention in tungsten exposed to low-energy pure and helium-seeded deuterium plasmas *J. Appl. Phys.* **109** 013309
[16] Ogorodnikova O.V. and Sugiyama K. 2013 Effect of radiation-induced damage on deuterium retention in tungsten, tungsten coatings and Eurofer *J. Nucl. Mater.* **442** 518–527
[17] Ogorodnikova O.V., Roth J. and Mayer M. 2008 Ion-driven deuterium retention in tungsten *J. Appl. Phys.* **103** 034902
[18] El-Atwani O., Gonderman S., Efe M., Gregory D.T., Morgan T., Bystrov K., Klenosky D., Qiu T. and Allain J.P. 2014 Ultrafine tungsten as a plasma-facing component in fusion devices: effect of high flux, high fluence low energy helium irradiation *Nucl. Fusion* **54** 083013
[19] Ackland G. 2010 Controlling radiation damage *Science* **327** 1587–8
[20] Grimes R.W., Konings R.J.M. and Edwards L. 2008 Greater tolerance for nuclear materials *Nat. Mater.* **7** 683–5
[21] Chimi Y., Iwase A., Ishikawa N., Kobiyama M., Inami T. and Okuda S. 2001 Accumulation and recovery of defects in ion-irradiated nanocrystalline gold *J. Nucl. Mater* **297** 355–7
[22] Zhang C.G., Zhou W.H., Li Y.G., Hu L. and Zeng Z. 2015 Anti-radiation mechanisms in nanoporous gold studied via molecular dynamics simulations *J. Nucl. Mater.* **466** 328–33
[23] Bai X.-M., Voter A.F., Hoagland R.G., Nastasi M. and Uberuaga B.P. 2010 Efficient annealing of radiation damage

near grain boundaries via interstitial emission *Science* **327** 1631–4
[24] Piaggi P.M., Bringa E.M., Pasianot R.C., Gordillo N., Panizo-Laiz M., del Río J., Gómez de Castro C. and Gonzalez-Arrabal R. 2015 Hydrogen diffusion and trapping in nanocrystalline tungsten *J. Nucl. Mater.* **458** 233–9
[25] Xiao W. and Geng W.T. 2011 Role of grain boundary and dislocation loop in H blistering in W: a density functional theory assessment *J. Nucl. Mater.* **430** 132–6
[26] Chen Z., Kecskes Laszlo J., Zhu K.G. and Wei Q.M. 2016 Atomistic simulations of the effect of embedded hydrogen and helium on the tensile properties of monocrystalline and nanocrystalline tungsten *J. Nucl. Mater.* **481** 190–200
[27] Valles G., Panizo-Laiz M., González C., Martin-Bragado I., González-Arrabal R., Gordillo N., Iglesias R., Guerrero C.L., Perlado J.M. and Rivera A. 2017 Influence of grain boundaries on the radiation-induced defects and hydrogen in nanostructured and coarse-grained tungsten *Acta Mater.* **122** 277–86
[28] El-Atwani O., Hattar K., Hinks J.A., Greaves G., Harilal S.S. and Hassanein A. 2015 Helium bubble formation in ultrafine and nanocrystalline tungsten under different extreme conditions *J. Nucl. Mater.* **458** 216–23
[29] El-Atwani O., Hinks J.A., Greaves G., Gonderman S., Qiu T., Efe M. and Allain J.P. 2014 *In situ* TEM observation of the response of ultrafine- and nanocrystalline-grained tungsten to extreme irradiation environments *Sci. Rep.* **4** 4716
[30] 't Hoen M.H.J., Dellasega D., Pezzoli A., Passoni M., Kleyn A.W. and Zeijlmans van Emmichoven P.A. 2015 Deuterium retention and surface modifications of nanocrystalline tungsten films exposed to high-flux plasma *J. Nucl. Mater.* **463** 989–92
[31] Valles G., González C., Martin-Bragado I., Iglesias R., Perlado J.M. and Rivera A. 2015 The influence of high grain boundary density on helium retention in tungsten *J. Nucl. Mater.* **457** 80–7
[32] Lu G.H., Zhou H.B. and Becquart C.S. 2014 A review of modelling and simulation of hydrogen behaviour in tungsten at different scales *Nucl. Fusion* **54** 086001
[33] Sun L., Jin S., Lu G.H. and Wang L.G. 2016 High hydrogen retention in the sub-surfaces of tungsten plasma facing materials: a theoretical insight *Scr. Mater.* **122** 14–7
[34] Becquart C.S. and Domain C. 2009 An object kinetic Monte Carlo simulation of the dynamics of helium and point defects in tungsten *J. Nucl. Mater.* **385** 223–7
[35] Becquart C.S., Domain C., Sarkar U., DeBacker A. and Hou M. 2010 Microstructural evolution of irradiated tungsten: *ab initio* parameterization of an OKMC model *J. Nucl. Mater.* **403** 75–88
[36] Xu Q., Sato K. and Yoshiie T. 2009 Interaction of tritium plasma and defects in tungsten irradiated with neutrons *J. Nucl. Mater.* **390–1** 663–6
[37] Heinola K. and Ahlgren T. 2013 Hydrogen retention to impurities in tungsten: a multi-scale study *J. Nucl. Mater.* **438** S1001
[38] Hu A. and Hassanein A. 2014 Modeling hydrogen isotope behavior in fusion plasma-facing components *J. Nucl. Mater.* **466** 56–62
[39] Ahlgren T., Heinola K., Vortler K. and Keinonen J. 2012 Simulation of irradiation induced deuterium trapping in tungsten *J. Nucl. Mater.* **427** 152–61
[40] Grigorev P., Matveev D., Bakaeva A., Terentyev D., Zhurkin Evgeny E., Van Oost G. and Noterdaeme J.-M. 2016 Modelling deuterium release from tungsten after high flux high temperature deuterium plasma exposure *J. Nucl. Mater.* **481** 181–89
[41] Ning R.H., Li Y.G., Zhou W.H., Zeng Z. and Ju X. 2012 Modeling D retention in W under D ions and neutrons irradiation *J. Nucl. Mater.* **430** 20–6
[42] Li Y.G., Zhou W.H., Huang L.F., Zeng Z. and Ju X. 2012 Cluster dynamics modeling of accumulation and diffusion of helium in neutron irradiated tungsten *J. Nucl. Mater.* **431** 26–32
[43] Hu L., Li Y.G., Zhang C.G. and Zeng Z. 2015 Cluster dynamics simulation of deuterium retention behaviors in irradiated beryllium *RSC Adv.* **5** 65750
[44] Ning R.H., Li Y.G., Zhou W.H., Zeng Z. and Ju X. 2012 An improved cluster dynamics model for hydrogen retention in tungsten *Int. J. Mod. Phys.* C **23** 1250042
[45] Li Y.G., Zhou W.H., Ning R.H., Huang L.F., Zeng Z. and Ju X. 2012 A cluster dynamics model for accumulation of helium in tungsten under helium ions and neutron irradiation *Commun. Comput. Phys.* **11** 1547–68
[46] Li Y.G., Yang Y., Short M.P., Ding Z.J., Zeng Z. and Li J. 2015 IM3D: a parallel Monte Carlo code for efficient simulations of primary radiation displacements and damage in 3D geometry *Sci. Rep.* **5** 18130
[47] Li Y.G., Yang Y., Short M.P., Ding Z.J., Zeng Z. and Li J. 2017 Ion radiation albedo effect: influence of surface roughness on ion implantation and sputtering of materials *Nucl. Fusion* **57** 016038
[48] Li S.Z., Li Y.G., Lo Y.C., Neerai T., Srinivasan R., Ding X.D., Sun J., Qi L., Gumbsch P. and Li J. 2015 The interaction of dislocations and Hydrogen-vacancy complexes and its importance for deformation-induced proto nano-voids formation in α-Fe *Inter. J. Plast.* **74** 175–91
[49] Surh M.P., Sturgeon J.B. and Wolfer W.G. 2004 Master equation and Fokker-Planck methods for void nucleation and growth in irradiation swelling *J. Nucl. Mater.* **325** 44–52
[50] Ghoniem N.M. and Sharafat S. 1980 A numerical solution to the Fokker–Planck equation describing the evolution of the interstitial loop microstructure during irradiation *J. Nucl. Mater.* **92** 121–35
[51] Petzold L. 1983 Automatic selection of methods for solving stiff and nonstiff systems of ordinary differential equations *SIAM J. Sci. Stat. Comput.* **4** 136–48
[52] Surh M.P., Sturgeon J.B. and Wolfer W.G. 2008 Void nucleation, growth, and coalescence in irradiated metals *J. Nucl. Mater.* **378** 86–97
[53] Dieter G.E. 1988 *Mechanical Metallurgy J. Franklin Inst.* **273** 766
[54] Skinner C.H. *et al* 2008 Recent advances on hydrogen retention in iter's plasma-facing materials: beryllium, carbon, and tungsten *Fusion Sci. Technol.* **54** 891–945
[55] Christien F. and Barbu A. 2009 Cluster dynamics modelling of irradiation growth of zirconium single crystals *J. Nucl. Mater.* **393** 153–61
[56] Derlet P.M., Nguyen-Manh D. and Dudarev S.L. 2007 Multiscale modeling of crowdion and vacancy defects in body-centered-cubic transition metals *Phys. Rev.* B **76** 054107
[57] Olsson P.A.T. 2009 Semi-empirical atomistic study of point defect properties in BCC transition metals *Comput. Mater. Sci.* **47** 135–45
[58] Liu Y.L., Zhang Y., Zhou H.B., Lu G.H., Liu F. and Luo G.N. 2009 Vacancy trapping mechanism for hydrogen bubble formation in metal *Phys. Rev.* B **79** 172103
[59] Becquart C.S. and Domain C. 2006 Migration energy of He in W revisited by *ab initio* calculations *Phys. Rev. Lett.* **97** 196402
[60] Becquart C.S. and Domain C. 2007 *Ab initio* calculations about intrinsic point defects and He in W *Nucl. Inst. Methods Phys. Res.* B **255** 23–6
[61] Watanabe Y. *et al* 2007 Formation of interstitial loops in tungsten under helium ion irradiation: rate theory modeling and experiment *Nucl. Inst. Methods Phys. Res.* B **255** 32–6
[62] Brailsford A.D., Bullough R. and Hayns M.R. 1976 Point defect sink strengths and void-swelling *J. Nucl. Mater.* **60** 246–56

[63] Heald P.T. and Harbottle J.E. 1977 Irradiation creep due to dislocation climb and glide *J. Nucl. Mater.* **67** 229–33
[64] Bullough R., Hayns M.R. and Wood M.H. 1980 Sink strengths for thin film surfaced grain boundaries *J. Nucl. Mater.* **90** 44–59
[65] Li X.Y., Liu W., Xu Y.C., Liu C.S., Fang Q.F., Pan B.C., Chen J.L., Luo G.N. and Wang Z.G. 2014 Principal physical parameters characterizing the interactions between irradiation-induced point defects and several tilt symmetric grain boundaries in Fe, Mo and W *J. Nucl. Mater.* **444** 229–36
[66] Wang K., Bannister Mark E., Meyer Fred W. and Parish Chad M. 2017 Effect of starting microstructure on helium plasma-materials interaction in tungsten *Acta Mater.* **124** 556–67
[67] Hardouin Duparc A., Moingeon C., Smetniansky de Grande N. and Barbu A. 2002 Microstructure modelling of ferritic alloys under high flux 1 MeV electron irradiations *J. Nucl. Mater.* **302** 143–55
[68] Jourdan T. and Crocombette J.-P. 2012 Rate theory cluster dynamics simulations including spatial correlations within displacement cascades *Phys. Rev.* B **86** 054113
[69] Fernandez N., Ferro Y. and Kato D. 2015 Hydrogen diffusion and vacancies formation in tungsten: Density Functional Theory calculations and statistical models *Acta Mater.* **94** 307–18
[70] Brailsford A.D. and Bullough R. 1981 The theory of sink strengths *Phil. Trans. R. Soc.* A **302** 87–137